OPTICA

# Intensity-preserving self-similar beams

Chenglong Wang,[1,2,†] Ronger Lu,[3,†] Ruizhi Zhao,[1,2,†] Jialing Li,[1,2] Miao Zhu,[1,2] Xuhui Sun,[1,2] Bing Gao,[1,2] Yibing Ma,[1,2] Chao Zhang,[1,2,4] Yiqiang Qin,[1,2,5] and Yanqing Lu[1,2,6]

[1]National Laboratory of Solid State Microstructures and Collaborative Innovation Center of Advanced Microstructures, Nanjing University, Nanjing 210093, China
[2]College of Engineering and Applied Sciences, Nanjing University, Nanjing 210093, China
[3]Department of Physics, Nanjing Tech University, Nanjing 211816, China
[4]zhch@nju.edu.cn
[5]yqqin@nju.edu.cn
[6]yqlu@nju.edu.cn
[†]These authors contributed equally to this work.

Received 26 September 2024; revised 22 December 2024; accepted 31 January 2025; published 14 February 2025

**Non-diffracting beams, propagating with unchanged transverse profiles and intensity, have been extensively studied in past decades. More recently, self-similar beams with scaling transverse profiles during propagation were proposed as a generalization of non-diffracting beams. Here, we present a type of beam that can be regarded as an intermediate mode between traditional self-similar beams and non-diffracting beams. During propagation, such beams feature a strict self-similar transverse profile and the intensity remains unchanged. Thus, we name these beams the "perfect self-similar beams". Our work reveals a class of previously unnoticed beam modes that hold both main characteristics of self-similar beams and non-diffracting beams, which conceptually expands the study of free-space beams with special propagation properties.** 

https://doi.org/10.1364/OPTICA.542980

As a long-known phenomenon, optical waves are always affected by diffraction, which entails beams, constituted of waves travelling in different directions, gradually broadening upon propagation. To satisfy the requirement of anti-diffraction characteristics of beams in the fields of free space communications, image forming, optical lithography, electromagnetic tweezers, etc., the development of techniques capable of reducing this phenomenon is of crucial importance. In 1987, Durnin proposed a class of monochromatic solutions to the Helmholtz equation, i.e., the Bessel beams, which feature an invariant transverse intensity profile while propagating forward [1,2]. The Bessel beams can be regarded as the superposition of a set of plane waves propagating in a cone, which have attracted extensive investigations and been employed for various applications [3–8]. By introducing the concept of Airy wave packets in quantum mechanics into optics, Airy beams, featuring a non-diffracting profile and parabolic trajectory, were proposed [9,10]. It has been demonstrated that Airy beams satisfy the paraxial Helmholtz equation and have special propagation properties such as self-acceleration and self-healing [11–14]. Other non-diffracting beams with different spatial structures, like Mathieu beams and parabolic beams, were also reported [15,16].

In addition, the self-similar evolution in physical systems is an ongoing research theme, especially in the area of nonlinear optics [17]. Back in 1992, some researchers found that the evolution of stimulated Raman scattering at long distances is dominated by the self-similar solutions, which depend on the combination $xt$ [18]. For the spatial case, a class of exact self-similar waves supported by inhomogeneous gain media was proposed in 2007 [19], of which the transverse profile retained a gradually narrowing parabolic shape even as the intensity continued to be amplified. More recently, by introducing coordinate transformation, self-similar waves in a linear system were proposed as the generalization of non-diffracting beams. Under the circular parabolic coordinate system, a beam mode called parabolic scaling Bessel beams can be obtained, of which the transverse profile scales parabolically during propagation [20]. Furthermore, by systematically studying the self-similar solutions of the paraxial Helmholtz equation, another two classes of self-similar beams whose scaling factors are linear and hyperbolic ellipses functions were proposed successfully [21]. Under tunable stretching transformations based on the Fresnel integral, the self-similar arbitrary-order Bessel-like beams can be obtained [22]. A more direct method for constructing arbitrary self-similar Bessel beams was proposed by using the transverse and longitudinal mapping principle of Bessel beams [23].

Unlike non-diffracting beams, these self-similar beams cannot preserve their intensities during propagation but vary along with the increase of the propagation distance. In fact, the self-similarity without intensity-preserving is not a surprising property of optical beams. As we know, Gaussian beams, the most commonly used eigenmodes of optical laser resonators, also have stable propagation with self-similarity. When propagating in free space, the beam waist of Gaussian beams stretches along the optical axis, leading to the scaling of the transverse profile and the decrease of the intensity along the optical axis [24]. As a generalization of non-diffracting beams, self-similar beams differ from non-diffracting beams in both the aspects of transverse profile and intensity.

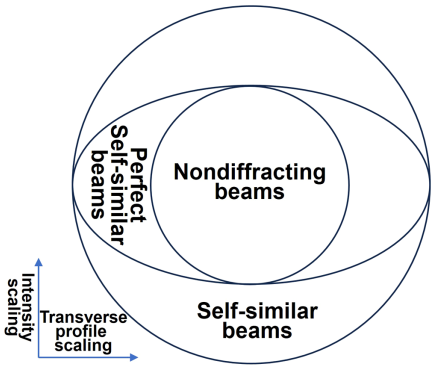


**Fig. 1.** Graphical representation of the relation of non-diffracting beams, self-similar beams, and perfect self-similar beams. The circle in the center denotes the non-diffracting beams with the unchanged transverse profile and intensity. The outer circle denotes the self-similar beams, of which the transverse profile and intensity both are scaling. The perfect self-similar beams are presented by the ellipse, whose transverse profile performs scaling while the intensity remains unchanged.

So, is there an intermediate beam mode whose transverse profile performs a scaling operation while the intensity remains unchanged during the propagation? Here, we present the discovery of intensity-preserving self-similar beams, which are exact solutions to the paraxial Helmholtz equation. The transverse profile of these beams features strict self-similarity along the propagating direction, while the intensity remains unchanged, which is significantly different from common self-similar beams. Thus we would like to call these beams the "perfect self-similar beams". In Fig. 1 we clarify the relation between non-diffracting beams, self-similar beams, and the newly presented perfect self-similar beams. We also analyze their properties when propagating in free space. Finally, we compare the perfect self-similar beams with the other two beams mentioned above.

We start with the two-dimensional (2D) case, considering a monochromatic light field propagating along the $z$ axis in free space with the wave vector $k$, and the complex amplitude can be represented by $U(x, z) = u(x, z)\exp(ikz)$. By taking $u$ into the 2D Helmholtz equation and using the paraxial approximation, we get the paraxial Helmholtz equation

$$\frac{\partial u}{\partial z} - \frac{i}{2k}\frac{\partial^2 u}{\partial x^2} = 0. \tag{1}$$

The variable substitution from $x$ to $x^2/z$ plays a key role in the deduction of the parabolic scaling Bessel beams [20], while the intensity profile of the resulted beams is still a function of the two variables, i.e., $x^2/z$ and $z$, which leads to the decrease of the intensity along the propagating direction. Thus, in this letter we further consider if there is a beam mode whose transverse intensity profile depends only on $x^2/z$. By introducing the intermediate variable $\xi = x^2/z$, and assuming $u(x, z) = A(\xi)$, Eq. (1) becomes an ordinary differential equation $(i + k\xi)A'(\xi) + 2i\xi A''(\xi) = 0$. Solving the equation, we get a beam mode described by the expression

$$u(x, z) = \mathrm{erf}\left(\sqrt{-\frac{ik}{2z}}x\right), \tag{2}$$

where $\mathrm{erf}(x) = (2\sqrt{\pi})\int_0^x e^{-\eta^2}\mathrm{d}\eta$ is the Gaussian error function. It can be seen that Eq. (2) is the unique solution with the form $u(x, z) = A(x^2/z)$ in the 2D case (the constant solution is ignored, which stands for the trivial solution of plane waves). The solution we proposed here has no extra parameter involved with $z$ outside the erf function, which sets it distinctly apart from the previously reported self-similar beams. According to this characteristic, when propagating from an arbitrary starting position $z_0$ to $z_1$, the transverse intensity profile can be described in principle by the function $I_1(x) = I_0(ax)$, where $x$ is the transverse coordinate, $I_0(x)$ stands for the starting state of position $z_0$, and the parameter $a$ therein denotes the scaling factor involved with propagation distance. For self-similar beams, the transverse intensity changes depending on $I_1(x) = CI_0(ax)$, of which the parameter $C$ is the intensity scaling factor involved with propagation distance. As for non-diffracting beams, the transverse intensity profile remains unchanged during the whole propagation process and can be described by $I_1(x) = I_0(x)$. For a better clarification, Fig. 2 schematically depicts the transverse intensity profiles of the three beams transmitting from $z_0$, with a common starting state $I_0(x)$, to the position of $z_1$.

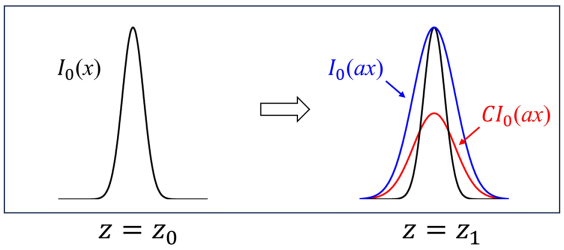


**Fig. 2.** A schematic of the transverse intensity profiles of (a) non-diffracting beams (in black), (b) self-similar beams (in red), and (c) perfect self-similar beams (in blue), propagating from an arbitrary starting position $z_0$ to $z_1$, with a common starting state.

Comparing the propagation characteristics of the three beams, we can find that the beam mode we present here has a self-similar transverse profile, while the intensity remains unchanged. With the properties of this beam mainly determined by the erf function, we call this beam the "erf beam". Obviously, the erf beam preserves its amplitude along curves $x^2/z = \mathrm{const}$, and sustains its transverse structure upon propagation, changing only in scale. From Eq. (2), the relation for the intensity distribution is calculated as $\hat{I}(x, z) \propto |\mathrm{erf}(\sqrt{-ik/2z}x)|^2$. In Fig. 3(a) we plot the intensity of the beam in the $xz$ plane with the wavelength of $\lambda = 1300$ nm (this wavelength, though arbitrary, is fixed throughout the present letter) and the transverse intensity profiles at $z = 100$ mm, $z = 50$ mm, and $z = 25$ mm are shown in Figs. 3(b), 3(c), and 3(d), respectively (for codes used for the pictures, see Supplement 1, as well as those for the following pictures). It can be seen that the three transverse intensity profiles at different distances are the same except for a transverse expanding operation, scaling by the square root of the propagation distance, which also can be predicted by the analytical expression of the erf beam. The expression depends only on the combination $x^2/z$, forcing the transverse profile to scale according to the parameter $1/\sqrt{z}$ and enabling the intensity to remain unchanged during propagation. This further illustrates that the erf beam is both intensity-preserving and self-similar at the same time.

The erf beam has an infinitely extended transverse width on any transmission cross section, which holds infinite energy. In practice, when generating beam modes with infinite energy, the apodization

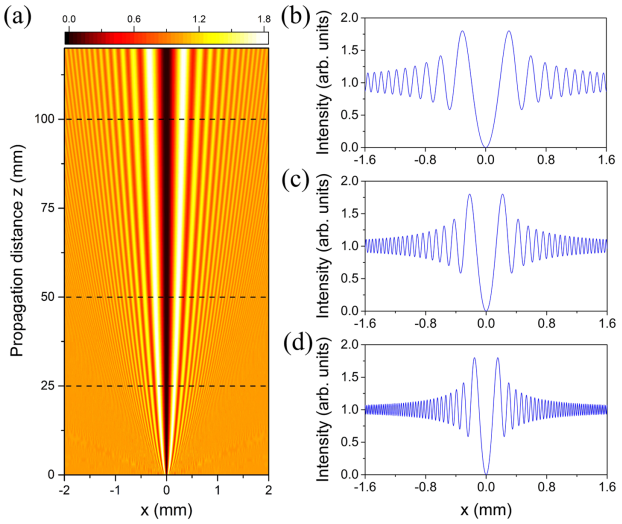


**Fig. 3.** (a) Transverse intensity profiles of the propagating erf beam. (b)–(d) Comparison of the transverse intensity profiles at (b) $z = 100$ mm, (c) $z = 50$ mm, and (d) $z = 25$ mm. In the profiles, we can find that two points, namely, $(x_1, z_1)$ and $(x_2, z_2)$, will have the exact same field distribution if their propagation distance $z$ and the transverse position $x$ satisfy ${x_1}^2/z_1 = {x_2}^2/z_2$. Thus, the erf beam has isointensity curves in the form of a series of parabolas with the same vertex.

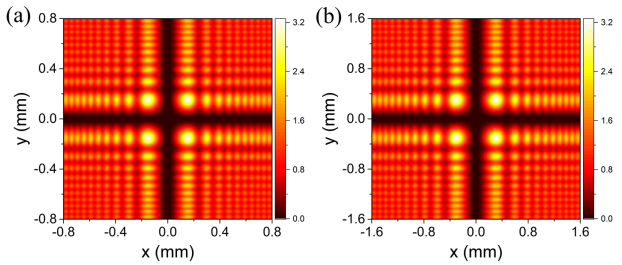


**Fig. 4.** Transverse intensity distribution patterns of a 3D erf beam at (a) $z = 25$ mm and (b) $z = 100$ mm. The intensity distribution patterns are the same in the two distances except for an expansion, which presents the intensity-preserving and self-similar properties of the beam.

method is often used [9,10]. Therefore, the total energy of the resulted beams is finite while the desirable features can survive over extended distances, and the law of conservation of energy is satisfied during propagation. From the transverse profiles, it can be seen that with the expansion of the profile, the number of the lobes in a certain horizontal distance decreases simultaneously, which means the expansion does not lead to the increasing of the total power but only the redistribution of it.

Similar to the construction method of the three-dimensional (3D) Airy beam, these results can be readily generalized in three dimensions; thus we have the 3D erf beam written as

$$u(x, y, z) = \mathrm{erf}\left(\sqrt{-\frac{ik}{2z}}x\right)\mathrm{erf}\left(\sqrt{-\frac{ik}{2z}}y\right), \tag{3}$$

which is also a solution to the paraxial Helmholtz equation. Figure 4 shows the transverse intensity profiles at the distances of $z = 25$ mm and $z = 100$ mm. Obviously, the transverse profile remains unchanged but performs a scaling operation, together with the analytical expression, which exactly illustrates the intensity-preserving and self-similar characteristics of the 3D erf beam.

The obtained 3D erf beam is just a particular solution in three dimensions; the general solution needs further discussion. To demonstrate this possibility, we consider a rotationally symmetric optical field with a spiral phase $\exp(in\varphi)$ in free space, of which $n$ is the topological charge, and the amplitude remains unchanged along the set of parabolic curves $\rho^2/z = \text{const}$. Thus, the complex amplitude can be described by $U(\rho, \varphi, z) = A(\rho^2/z)\exp(ikz)\exp(in\varphi)$. Taking $u(\rho, \varphi, z) = A(\rho^2/z)\exp(in\varphi)$ and inserting $u$ into the 3D Helmholtz equation, under the paraxial approximation, we have the 3D paraxial Helmholtz equation in cylindrical coordinates:

$$\frac{\partial u}{\partial z} - \frac{i}{2k}\left(\frac{\partial^2 u}{\partial \rho^2} + \frac{1}{\rho}\frac{\partial u}{\partial \rho} + \frac{1}{\rho^2}\frac{\partial^2 u}{\partial \varphi^2}\right) = 0. \tag{4}$$

Here we focus on the case of beams with $n = 1$. By introducing the intermediate variable $\xi = \rho^2/z$, Eq. (4) becomes an ordinary differential equation: $A(\xi) + (2ik\xi^2 - 4\xi)A'(\xi) - 4\xi^2 A''(\xi) = 0$. Solving the equation, the beam can be found for this case in an analytical form:

$$u(\rho, \varphi, z) = \sqrt{\frac{k\rho^2}{z}}\exp\left(\frac{ik\rho^2}{4z}\right)\left\{C_1\left[-J_0\left(\frac{k\rho^2}{4z}\right) + iJ_1\left(\frac{k\rho^2}{4z}\right)\right] + C_2\left[K_0\left(-\frac{ik\rho^2}{4z}\right) - K_1\left(\frac{ik\rho^2}{4z}\right)\right]\right\}\exp(i\varphi), \tag{5}$$

where $C_1$ and $C_2$ are constant, $J_n$ denotes $n$th-order Bessel function, and $K_n$ stands for $n$ th-order Hankel function of imaginary argument ($n = 0$, 1). We see that Hankel functions $K_0$ and $K_1$ diverge at the origin, which should be discarded. Taking $C_1 = \sqrt{\pi/8}$, we can express Eq. (5) in the simpler form as

$$u(\rho, \varphi, z) = \sqrt{\frac{\pi k\rho^2}{8z}}\exp\left(\frac{ik\rho^2}{4z}\right)\left[-J_0\left(\frac{k\rho^2}{4z}\right) + iJ_1\left(\frac{k\rho^2}{4z}\right)\right] \times \exp(i\varphi). \tag{6}$$

Obviously, this field results from the summation of two Bessel-type beams. From Eq. (6) it can be seen that the optical field will preserve its spatial structure because the function $u(\rho, \varphi, z)$ therein depends only on the combination of variables $\rho^2/z$, while the Bessel beams match the function $J_n(\alpha\rho)$ and strictly maintain the transverse profile in any plane orthogonal to the propagating direction. Utilizing asymptotic expansions of Bessel functions $J_0$ and $J_1$, it can be proved that when $z \to 0$, the optical field determined by Eq. (6) turns into a uniform-intensity field $\exp(i\varphi)$, which conforms to the complex transmittance of the spiral phase plate with the first-order phase singularity ($n = 1$). Thus, the optical field described by Eq. (6) can be easily formed behind a first-order spiral phase plate illuminated by a plane wave, which has been displayed by previous publications, wherein the cases of different topological charge indices with similar analytical expressions are also concerned [25,26]. Here we focus on the characteristics of the beam. Figure 5 shows two transverse intensity profiles at the distances of $z = 25$ mm [Fig. 5(a)] and $z = 100$ mm [Fig. 5(c)] and their corresponding intensity distribution patterns [Figs. 5(b) and 5(d)]. It can be seen that the two transverse profiles overlap completely after stretching the horizontal coordinate of Fig. 5(a).

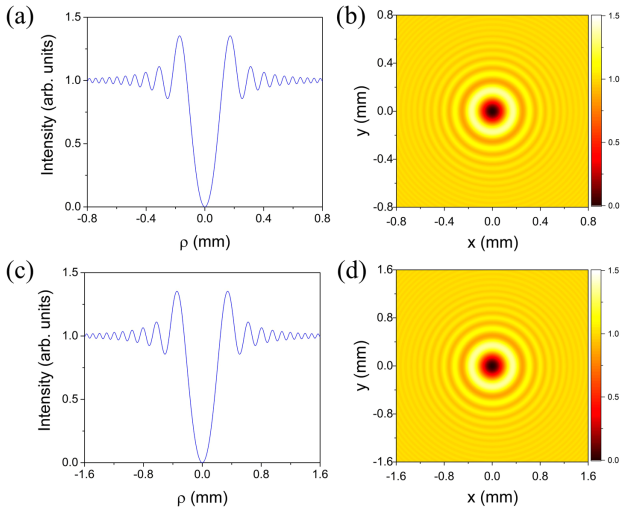


**Fig. 5.** Transverse intensity profiles of the perfect self-similar beam (3D case in cylindrical coordinates) are strictly similar at the distances of (a) $z = 25$ mm and (c) $z = 100$ mm and the intensity remains unchanged. (b), (d) Their corresponding intensity distribution patterns, which also show the intensity-preserving and self-similar properties of the beam.

Similarly, any two points that satisfy $\rho_1^2/z_1 = \rho_2^2/z_2$, namely, on the same paraboloid $\rho^2/z = C$, will have the same field distribution. And the intensity does not change during propagation too. From the intensity profiles and its analytical expression, we confirm that this beam belongs to the class of perfect self-similar beams.

By now, we have obtained several perfect self-similar beams in both two and three dimensions. It is worth comparing comprehensively the features of the perfect self-similar beams with the other two types of beams.

We first compare the perfect self-similar beams with the non-diffracting beams to explain the self-similar property of the former. These two kinds of beams both maintain their intensity during the propagation. The difference is that the transverse intensity profiles are directly congruent for the Bessel beams and other non-diffracting beams, while congruent only after certain scaling operation for the perfect self-similar beams. We also find that every non-diffracting beam has a series of isointensity curves. The isointensity curves are a series of parallel straight lines for the Bessel beams and other non-diffracting beams, a series of parallel parabolas for the Airy beams, and a series of parabolas with the same vertex for the perfect self-similar beams. In short, when comparing with these non-diffracting beams, what makes the perfect self-similar beams special is that while maintaining the unchanged intensity during propagation, they get a gradually broadening transverse profile, which is the so-called self-similarity.

As for self-similar beams, the most significant difference between these beams and the perfect self-similar beams is that the beam shape broadens during the propagation process, and the intensity is decreased. While the perfect self-similar beams we proposed in this letter broaden in the propagation process, the intensity remains unchanged. The same goes for the parabolic self-similar beams and other self-similar beams with different scaling factors, presenting a decreasing intensity, which differentiates them from the beams we proposed, and thus we term our intensity-preserving self-similar beams as "perfect self-similar".

In conclusion, by solving the paraxial Helmholtz equation, we demonstrate a class of beams whose transverse profile scales parabolically during propagation while the intensity can be maintained, and the analytical expressions are obtained both in two and three dimensions. These beams can be regarded as the intermediate mode between non-diffracting beams and self-similar beams. Our results conceptually expand special beam modes in free space and would be of benefit for exploring applications in free space communications, optical imaging, optical micromanipulation, etc. And it may also be extended to acoustics, fluids, or other relevant systems.

**Funding.** National Key Research and Development Program of China (2022YFA1205100, 2022YFA1405000); National Natural Science Foundation of China (12474327, 12274214, 12004177); Natural Science Foundation of Jiangsu Province (BK20200701).

**Disclosures.** The authors declare no conflicts of interest.

**Data availability.** Data underlying the results presented in this paper are not publicly available at this time but may be obtained from the authors upon reasonable request.

**Supplemental document.** See Supplement 1 for supporting content.

## REFERENCES

1. J. Durnin, J. Opt. Soc. Am. A **4**, 651 (1987).
2. J. Durnin, J. J. Miceli, and J. H. Eberly, Phys. Rev. Lett. **58**, 1499 (1987).
3. T. Wulle and S. Herminghaus, Phys. Rev. Lett. **70**, 1401 (1993).
4. S. P. Tewari, H. Huang, and R. W. Boyd, Phys. Rev. A **54**, 2314 (1996).
5. R. Piestun and J. Shamir, J. Opt. Soc. Am. A **15**, 3039 (1998).
6. V. Garcés-Chávez, D. McGloin, H. Melville, *et al.*, Nature **419**, 145 (2002).
7. D. McGloin and K. Dholakia, Contemp. Phys. **46**, 15 (2005).
8. A. S. Rao, Phys. Scripta **99**, 062007 (2024).
9. G. A. Siviloglou, J. Broky, A. Dogariu, *et al.*, Phys. Rev. Lett. **99**, 213901 (2007).
10. G. A. Siviloglou and D. N. Christodoulides, Opt. Lett. **32**, 979 (2007).
11. T. Vettenburg, H. I. C. Dalgarno, J. Nylk, *et al.*, Nat. Methods **11**, 541 (2014).
12. Y. Lumer, L. Drori, Y. Hazan, *et al.*, Phys. Rev. Lett. **115**, 013901 (2015).
13. N. K. Efremidis, Z. Chen, M. Segev, *et al.*, Optica **6**, 686 (2019).
14. M. Yaalou, Z. Hricha, and A. Belafhal, Opt. Quant. Electron. **55**, 138 (2022).
15. J. C. Gutiérrez-Vega, M. D. Iturbe-Castillo, and S. Chávez-Cerda, Opt. Lett. **25**, 1493 (2000).
16. M. A. Bandres, J. C. Gutiérrez-Vega, and S. Chávez-Cerda, Opt. Lett. **29**, 44 (2004).
17. J. M. Dudley, C. Finot, D. J. Richardson, *et al.*, Nat. Phys. **3**, 597 (2007).
18. C. Menyuk, D. Levi, and P. Winternitz, Phys. Rev. Lett. **69**, 3048 (1992).
19. S. A. Ponomarenko and G. P. Agrawal, Opt. Lett. **32**, 1659 (2007).
20. N. Gao and C. Xie, Opt. Lett. **39**, 3619 (2014).
21. N. Gao and C. Xie, Opt. Lett. **40**, 1216 (2015).
22. M. Goutsoulas, D. Bongiovanni, D. Li, *et al.*, Opt. Lett. **45**, 1830 (2020).
23. Y. Li, Y. Zou, Z. Guo, *et al.*, Chin. Opt. Lett. **22**, 022601 (2024).
24. C. Alpmann, M. Boguslawski, P. Rose, *et al.*, Proc. SPIE **8274**, 82740R (2012).
25. V. V. Kotlyar, A. A. Almazov, S. N. Khonina, *et al.*, J. Opt. Soc. Am. A **22**, 849 (2005).
26. S. N. Khonina, V. V. Kotlyar, M. V. Shinkaryev, *et al.*, J. Mod. Opt. **39**, 1147 (1992).